HHS Public Access

Author manuscript

Ann Biomed Eng. Author manuscript; available in PMC 2021 February 20.

Published in final edited form as:

Ann Biomed Eng. 2019 September ; 47(9): 1960–1970. doi:10.1007/s10439-019-02321-1.

The Influence of Shear Anisotropy in mTBI: A White Matter Constitutive Model

FATMA A. MADOUH[1], **K. T. RAMESH**[1,2]

[1]Department of Mechanical Engineering, Johns Hopkins University, Baltimore, MD, USA

[2]Hopkins Extreme Materials Institute, Johns Hopkins University, Baltimore, MD, USA

Abstract

We examine the influence of shear anisotropy of brain tissue on the potential for mild traumatic brain injury. First we develop a new constitutive description for the white matter in the brain that can capture the anisotropic behavior of the white matter in both tension and shear. The material parameters for the models are determined using a set of three experiments already published in the literature. The calibrated and parameterized model is then implemented in a computational (finite element) model of the head. This computational model is two-dimensional and is used to simulate a previously published injury-causing event in the National Hockey League, using axonal strain as criterion to assess the level of diffuse axonal injury. It is demonstrated that the inclusion of shear anisotropy affects both the nature and the extent of predicted injury. Further, the locations of the predicted injury are more consistent with observations in the literature.

Keywords

Shear anisotropy; Constitutive-model; TBI; Injury

INTRODUCTION

Traumatic Brain Injury (TBI)[1] is typically caused by a sudden mechanical loading to the head such as that resulting from a fall, a blast or a car crash. The level of injury is classified as mild, moderate or severe depending on the degree and nature of damage to the brain. More than 82% of military TBI in the years 2000–2017 were mild, and hence greater efforts are typically focused towards mild TBI (mTBI).[8] It is difficult to properly diagnose mTBI and the corresponding damage in the brain at the acute stages of injury, due to a lack of abnormalities in standard medical imaging immediately after an mTBI-causing event. In this context, computational simulations offer some hope for both understanding and early diagnosis of mTBI.

Address correspondence to K. T. Ramesh, Department of Mechanical Engineering, Johns Hopkins University, Baltimore, MD, USA. ramesh@jhu.edu.

CONFLICT OF INTEREST

The authors have no conflict of interest to declare.

[1]Source: Center for Disease Control and Prevention http://www.cdc.gov/traumaticbraininjury/data/rates.html.

Finite element models are often used as computational tools to study mTBI and estimate injury in humans. These models are either two dimensional (2D)[31,42,43] or three dimensional (3D) models,[3,5,11,29,30,39,45] and differ greatly in the anatomical details that are considered, ranging from low to high fidelity.

Most early TBI computations treated brain tissue as isotropic material.[9,17,36,45,47] With the discovery of the brain's fiber network, some TBI models have used anisotropic descriptions for the white matter and isotropic descriptions to represent gray matter.[37,42,43] The anisotropic models have been developed by using both continuum(e.g. Ref. 26) or structural (e.g. Ref. 19) approaches. However, all of the TBI models to date have accounted for anisotropy in tension but not in shear, despite clear evidence of shear anisotropy in white matter.[13]

In this work we present a material model for white matter that captures anisotropy in both tension and shear. The material parameters are determined by calibration with respect to data from the literature and the calibrated model is then validated against live human data in a non-injurious context. The validated model is then used to simulate a specific National Hockey League (NHL) incident that resulted in injury. In order to demonstrate the role of shear anisotropy in mTBI modelling, the results of the new material model are compared to the results obtained with model that includes only tension anisotropy.

MATERIALS AND METHODS

The materials in brain tissue are typically separated into two types: white matter and gray matter. The gray matter primarily consists of neuronal cell bodies and is typically modeled as an isotropic material. On the other hand, the white matter is largely composed of axons surrounded by various types of glial cells forming a network of fiber bundles. The existence of this network causes the material to have a different response if stretched parallel to the fiber direction than if stretched perpendicular to the fiber direction.[37] A similar anisotropy applies to the shear response.[13] Thus, white matter is an anisotropic material in both tension and shear. In this section, a constitutive model for white matter is described which includes both modes of anisotropy.

Constitutive Model

We start with a simple volume of material with fibers in one direction. The initial fiber direction $\mathbf{a}_0$ in the reference configuration and the new fiber vector $\mathbf{a}$ in the deformed configuration are related through the deformation gradient $\mathbf{F}$ and the fiber stretch λ by

$$\mathbf{F}\mathbf{a}_0 = \lambda \mathbf{a}\,. \tag{1}$$

The strain energy function for a transversely isotropic material is usually represented using three invariants for the isotropic response of the material,

$$I_1 = tr\mathbf{C}, I_2 = \frac{1}{2}\left[(tr\mathbf{C})^2 - \mathbf{tr}\left(\mathbf{C}^2\right)\right], \tag{2}$$

and two pseudo-invariants for the anisotropic response[33]

$$I_4 = \mathbf{a}_0 \cdot \mathbf{C} \cdot \mathbf{a}_0 = \lambda^2 \text{ and} \tag{3}$$

where **C** is the Right Cauchy–Green tensor. Note while I_4 depends only on the fiber stretch, I_5 carries information about both fiber stretch and fiber-matrix interaction.[12] Since white matter is a nearly incompressible material and the model will be used in a finite element computation, the strain energy function is assumed to be partitioned to avoid shear locking, so that

$$W = W_{Volumetric} + W_{Isochoric} \tag{4}$$

where $W_{Volumetric}$ is the strain energy part allowing volume change and $W_{Isochoric}$ captures deformation without any change in volume. The deformation gradient tensor F is modified to

$$\mathbf{F} = \mathbf{J}^{\frac{1}{3}}\overline{\mathbf{F}} \tag{5}$$

where $J = \det\mathbf{F}$ is the volume ratio ($W_{Volumetric} = f(J)$) and $\overline{\mathbf{F}}$ is the deformation gradient with constant volume $\left(W_{Isochoric} = f(\overline{\mathbf{F}})\right)$. Accordingly the invariants $\overline{I_i}$ are expressed in terms of the modified Cauchy–Green tensor $\overline{\mathbf{C}} = \overline{\mathbf{F}}^T\overline{\mathbf{F}}$. We now assume that the isochoric strain energy, $W_{Isochoric}$, is composed of two parts, one representing the isotropic response of white matter (assumed to be Neo-Hookean) and the other representing the fiber reinforcement:

$$W_{Isochoric} = W_{Isotropic} + W_{Anisotropic} \tag{6a}$$

$$W_{Isotropic} = C_1\left(\bar{I}_1 - 3\right) \tag{6b}$$

$$W_{Anisotropic} = C_2\left(\bar{I}_4 - 1\right)^2 + C_3\left(\bar{I}_5 - \bar{I}_4^2\right) \tag{6c}$$

where C_1, C_2 and C_3 are material parameters. The $W_{Anisotropic}$ incorporates anisotropy in both tension and shear, and $\bar{I}_1$, $\bar{I}_4$ and $\bar{I}_5$ are defined analogously to I_1, I_4 and I_5 when **F** is replaced by $\overline{\mathbf{F}}$. Note that the second term in Eq. (6c) represents the fiber-matrix interaction only. The values of the material parameters C_1, C_2 and C_3 can be determined (e.g.) from three experiments:

1. Tension perpendicular to the fibers to obtain C_1 since this mode is dominated by the matrix response to deformation.
2. Tension along the fiber direction to obtain C_2 (mode dominated by the fiber stretch contribution).
3. Shear perpendicular to the fibers to obtain C_3 (mode dominated by the fiber-matrix shear interaction).

We note that, to our knowledge, previous mTBI anisotropic white matter models have not accounted for the fiber-matrix interactions and I_5 in the formulation.

Finally, the volumetric part of the strain energy is described in terms of the volume ratio J and the bulk modulus K, as is widely used in other studies for white matter[4,5,11]

$$W_{Volumetric} = \frac{K}{2}\left(\frac{J^2-1}{2} - \ln J\right) \tag{7}$$

With these definitions of the strain energy, the constitutive equation of white matter can be derived following[12] with the Cauchy stress tensor $\boldsymbol{\sigma}$ related to the strain energy density by

$$\begin{aligned}\sigma = \frac{2}{J}\Bigg\{ & \bar{I}_3\frac{\partial W}{\partial \bar{I}_3}\mathbf{I} + \left(\frac{\partial \mathbf{W}}{\partial \bar{\mathbf{I}}_1} + \bar{\mathbf{I}}_1\frac{\partial \mathbf{W}}{\partial \bar{\mathbf{I}}_2}\right)\bar{\mathbf{b}} - \frac{\partial \mathbf{W}}{\partial \bar{\mathbf{I}}_2}\bar{\mathbf{b}}^2 \\ & + \bar{I}_4\frac{\partial W}{\partial \bar{I}_4}\mathbf{a}\otimes\mathbf{a} + \bar{\mathbf{I}}_4\frac{\partial \mathbf{W}}{\partial \bar{\mathbf{I}}_5}(\mathbf{a}\otimes\bar{\mathbf{b}}\mathbf{a} + \mathbf{a}\bar{\mathbf{b}}\otimes\mathbf{a})\Bigg\}\end{aligned} \tag{8}$$

where $\mathbf{I}$ is the identity tensor and $\bar{\mathbf{b}} = \bar{\mathbf{F}}\bar{\mathbf{F}}^{\mathbf{T}}$ is the modified Left Cauchy–Green tensor.

To understand the effects of the shear anisotropy (I_5), we compare our results to those obtained using an anisotropic model without shear anisotropy: the Holzapfel–Gasser–Ogden (HGO) model which was used by Wright *et al.*[42] For a single family of fibers in a representative volume, the HGO model used by Ref. 42 was:

$$\begin{aligned} W_{Isotropic} &= C_1\left(\bar{I}_1 - 3\right), \\ W_{Anisotropic} &= \frac{k_1}{2k_2}\left\{e^{k_2(\bar{E})^2} - 1\right\}, \end{aligned} \tag{9}$$

where $\bar{E} = \kappa\left(\bar{I}_1 - 3\right) + (1-3\kappa)\left(\bar{I}_4 - 1\right)$, k_1 is a parameter representing tension anisotropy, k_2 is a scaling factor and k is the fiber dispersion parameter. Note that the special case of $k = 0$ and a single fiber family and for small k_2 (as in Wright *et al.*[42]), Eq. (9) reduces to the same form as Eq. (6) with $C_3 = 0$ (i.e., only the $\bar{I}_4$). The major difference between our model (Eq. 6) and the HGO model (Eq. 9) is the following: our model accounts for tension and shear anisotropy but fiber dispersion is not included, while the HGO model accounts for tension anisotropy and includes fiber dispersion but no shear anisotropy. Both models include fiber-induced anisotropy, but the HGO model allows the fiber directions to vary somewhat (depending on the dispersion).

Material Properties

Now that we have defined the constitutive models, we need to determine the parameters C_1, C_2 and C_3 of Eq. (6), k_1, k_2 and k of Eq. (9) and the bulk modulus K of Eq. (7). Parameters for Eq. (9) were taken directly from Wright *et al.*[42] (Table 1). The bulk modulus K is chosen to be 2.19 GPa, consistent with some (but by no means all) of the prior literature for TBI computations.[34,40,44]

Since we expect the brain tissue to be strain-rate dependent,[2,10,35] we incorporate viscoelastic effects through a Prony series (described in the next subsection). For this particular implementation, C_1, C_2 and C_3 should be determined from low strain rate data of tension and shear experiments performed with respect to the dominant fiber direction, and there are few studies that have this information. Jin *et al.*[13] examined tissues from four regions of human adult brains: Cortex, Thalamus, Corpus Callosum and Corona Radiata. Compression, tension and shear tests with respect to fiber direction were performed for all four regions using three strain rates (0.5, 5 and 30 s^{-1}). An attempt to fit all the material parameters to the 0.5 s^{-1} strain rate data (lowest strain rate in Jin's *et al.*[13] dataset) results in a negative value for C_3, which is not allowed in this hyperelastic model. It is possible that there are variations in the experimental data because of effects such as the long post-mortem time of the samples (averaging 4 days post mortem) or the fact that each test direction was performed on a different subject (gender and age differed, the latter ranging from 48 to 94 years). The net result is that we can not use the three tests of the low strain rate (0.5 s^{-1}) in Jin's *et al.*[13] experiment to determine the full set of C_1, C_2 and C_3. Instead we consider Velardi *et al*'s.[37] work. They performed tensile tests on fresh adult porcine brain tissue from three different regions: Cortex, Corpus Callosum (CC) and Corona Radiata (CR) at a strain rate of 0.1 s^{-1}. For both CC and CR, tension tests were performed both parallel and perpendicular to the fibers allowing us to obtain C_1 and C_2 [Fig. 1 (top and middle, respectively)]. However, Velardi *et al.*[37] did not perform shear testing with respect to the fiber direction. To obtain C_3, therefore, we used the work of Jin *et al.*[13] The parameter C_3 is determined by fitting the Jin *et al.*[13] results for shear perpendicular to the fiber direction [Fig. 1 (bottom)]. A nonlinear least squares method was used for all parameters, which are shown in Table 1, and the corresponding R^2 values are above 0.9 for the three parameters. Since both experimental studies[13,37] we used for the fitting are performed under low strain rate loading (0.1 and 0.5 s^{-1} respectively), we consider the fitted parameters to define the long-term response of the material. The viscoelastic modulus behavior will be described in the next subsection.

Given the availability of data, we have had to mix two tissue sources (porcine and human) when obtaining our parameters. Prange and Margulies[27] compared the properties of porcine and human brain tissue, and found that human brain tissue was stiffer than the porcine tissue. On the other hand, Nicolle *et al.*[25] obtained shear viscoelastic material properties for porcine tissue, compared them to human tissue properties reported in the literature, and concluded that porcine tissue stiffnesses were within the range of human tissue stiffnesses. Similarly, Nicolle *et al.*[24] found no difference in the material properties of the brain tissue between the two species. In this context of the data in the available literature, we believe that using two different tissue sources to calibrate our model is reasonable.

Finite Element Head Model

Our finite element (FE) head model is based on magnetic resonance image (MRI) data of a healthy human.[42] For simplicity, and to provide insights into when building and running a more realistic but much more expensive 3D simulation is necessary (such simulations are underway), we consider three 2D slices (extracted from the 3D MRI), one for each plane: axial, coronal and sagittal. Each slice is segmented for the following brain structures when

appropriate: skull, dura (with falx and tentorium), cerebro-spinal fluid (CSF), gray matter, white matter, cerebellum, bridging veins and ventricles (Fig. 2).

The shear anisotropic model described in the previous section is used for white matter, with the primary fiber bundle direction assigned by co-registering the MRI with Diffusion Tensor Imaging (DTI) of the same subject, with the dominant direction of the fiber bundle for each voxel recorded. Since gray matter does not have a preferred orientation, we used Eq. (9) with the fiber dispersion k set to 1/3 for gray matter. Since the brain tissue mechanical behavior is dependent on the strain rate,[7,10,28,35] we adapted a one-term Prony series shear modulus to compensate for the strain rate effect from Wright *et al.*[42] The calibrated shear modulus ($2C_1$) is considered as the long-term shear modulus, and using a commonly reported ratio long-term and short-term moduli[42,46] the value of the long-term modulus is extracted. Table 2 summarizes the material models for all other structures.

All other details about the material models and properties used for each structure (other than what we derived here for the white matter) may be obtained from Wright *et al.*,[42] which we use as a benchmark. Both our computational simulations and Wright *et al.*[42] are two dimensional with identical head structure and mesh (identical element types as well–both three (CPE3) and four (CPE4R) node plane strain elements were used in the mesh, with reduced integration procedures described in the Abaqus documentation) and simulations are performed using the explicit Abaqus commercial software simulations (Dassault Systémes Simulia Corp., Providence, RI). Validation of both models is performed using an *in-vivo* brain deformation experiment on a human subject (covered in the next subsection). In this way, we focus on the effects of shear anisotropy and eliminate all other sources that could produce differences in the results.

Since finite element calculations can be affected by the mesh size, we conducted a mesh sensitivity analysis. A constant angular acceleration is applied to three mesh sizes: (1) Fine mesh with max element size of 1 mm (2) Medium mesh with max element size of 2 mm (3) Coarse mesh with max element size of 4 mm. For the medium and coarse meshes, elements were a combination of four and three node plane strain elements while the fine mesh is composed of only four node plane strain elements (by converting MRI voxels directly to elements). For each mesh, we examine the evolution of the area fraction of white matter that has been deformed to axonal strains (strain along the fiber direction) greater than some threshold (Fig. 3 shows the mesh convergence results for one of the examined thresholds, which is 15%). For all strain thresholds/levels, we observe that the difference between the fine and medium meshes is smaller than the difference between medium and coarse meshes. We have also examined convergence with respect to the locations of the largest damage. Given this convergence, we selected the medium mesh for the results presented here.

Validation of the Head Model for Non-Injurious Loading

Accurate modelling of the brain tissue is a key factor in determining the level of injury during traumatic events. We validate our head model by simulating the *in-vivo* brain rotational motion experiment of Knutsen *et al.*[18] Volunteers with no history of brain injury used a device that induces a non-injurious rotation about the horizontal/axial plane of the head inside the MRI at Henry Jackson Foundation (HJF). The tagged MRI technique was

then used to extract the 3D brain motions. The acceleration profile obtained from the experiment is applied to the axial slice of our model, and the resulting computed shear strains are compared to the experimental values.

Figure 4 shows the computed shear strains in the axial slice from our shear anisotropic model (Eq. 6) and from the HJF experiment at four times. These times are based on the experimental data, which were collected and processed every 18 ms, beginning 9 ms after the loading. The evolution of shear strain is captured by the model in the following senses. After 45 ms, both the experiment and the model have the maximum shear strains reaching the middle of the brain, indicating consistent shear wave speed, and the locations of maximum and minimum strains are generally consistent between the simulation and the experiment.

To quantify this full field spatial validation for the model, we examine the statistical level of agreement using four different tests discussed by Ganpule *et al.*[11]: (1) index of agreement (d_r) (2) coefficient of efficiency (E_2) (3) root mean squared error (RMSE) to observations standard deviation Ratio (RSR) and (4) correlation score (CS) (Table 3). For these statistical measures, we define the measured shear strains from the HJF experiment as the observed data O_i, and the results from our shear anisotropic model simulation as the predicted data P_i. Table 4 shows the results of all the statistical measures. For d_r;[41] E_2[20] and RSR,[23] the results are closer to the "better" end of the range (the upper end for d_r and E_2 and the lower end for RSR). Unfortunately, these particular metrics do not yet have a defined "level of goodness". For the CS results, the first two time frames (27 and 45 ms) are classified as fair agreement while the last two time frames (63 and 81 ms) are classified as marginal agreement.[14] However, since our model is intended to be used for injurious loading which typically lasts between 15 and 36 ms, we find the overall statistical results to be acceptable.

The simulation, of course, has some advantages over the experiment: higher temporal resolution and higher structural resolution. While the experimental data is available only every 18 ms, the simulation data can be extracted with much finer resolution, e.g. every millisecond. Since injurious loading usually lasts from 15 to 30 ms, the simulation produces a finer sense of the evolution of strains. Moreover, the experiment does not capture strains within the ventricles, which could affect the calculated strains in the surrounding tissues. We note also that Knutsen *et al.*[18] eliminated rigid body rotation only at the first part of the experiment (before the head stops completely by 3–4 degrees), but did not correct for rigid body motion afterwards. Other discrepancies between the experiment and the simulation could arise from structural differences between the subject heads in the experiment and the computation, or the large spacing of the experimental tag lines in comparison with simulation element size (8 mm as compared to 1–2 mm).

Injury Criteria

Defining an injury threshold for mTBI remains very difficult. No single injury threshold has yet been globally accepted. The difficulty arises because of the contribution of so many factors in any traumatic event, including but not limited to: location of impact (if any), direction of motion, rotational and translational accelerations, duration of the event, nature of the subject's neck, age and so forth. Accordingly multiple biomechanical thresholds have

been used in the literature such as coup and contrecoup pressure,[38] von Mises stress,[16] principal strains,[16] strain rate[15] and axonal strains.[42] Since our new model is intended to better describe the white matter tissue, we selected the axonal strain injury threshold. Bain and Meaney[1] tested the optic nerves of guinea pigs at starin rates of 30–60 s^{-21} and suggested an optimal threshold for axonal strain injury of 18% (Note: the simulations in our study use strain rates of 25 s^{-21} based on the time of onset of damage). In our simulations (using both models), the elements are only labeled as "injured" once they reach or exceed the injury threshold of axonal strain ≥ 18%. They continue to carry load and to deform after the threshold, but once identified as injured, they remain labeled as injured throughout the simulation even if the axonal strain decreases in the next timesteps.

An Injurious Event

We now assign the known injury-causing loading conditions for each model/orientation (sagittal, coronal and axial). A reconstructed NHL incident previously used by Wright *et al.*[42] is examined, so as to directly compare model results. For each orientation, the corresponding linear and angular accelerations are applied in explicit FE simulations. Since the known loading curves[42] have a duration of only 15 ms and cutoff at non-zero values, we extend the curves so that the acceleration magnitudes are linearly decreased to zero over 5 ms (and remain zero thereafter). However, the total simulation time is determined by the time needed for shear wave propagation inside the brain.[11] The simulations are stopped when the damage of white matter ceases to evolve (change in damage of 0.25% or less for three consecutive milliseconds) in all loading cases.

RESULTS

The shear anisotropy simulation results for the injury case are presented in Fig. 5a in terms of the axonal strain (damage) distributions in the three cross-sections. The degree of damage in each case is quite different from that previously obtained by Wright *et al.*[42] using the HGO model with only tension anisotropy.

The injury levels predicted by the two models are compared in Fig. 5b. Red areas in the figure indicate elements of white matter in which the axonal strain reached or exceeded the injury threshold of 18% (any element that fulfills the injury criterion is considered damaged for the rest of the simulation). Overall, the damage predicted by the shear anisotropic model is clearly higher than the HGO model predictions.

Beside comparing damage location, the area of damage in each slice was also investigated. The percentage of damaged area Ω, is calculated as

$$\Omega = \frac{\int_{A_{WM}} A_{\varepsilon_{Axon} \geq 18\%} dA}{\int_{A_{WM}} A dA} \times 100 \quad (10)$$

where $A_{\varepsilon_{Axon} > 18\%}$ is area of white matter elements with axonal strain exceeding 18% and A_{WM} is the white matter area.

Using Eq. (10), the percent damage for each slice predicted by both models are calculated. In the axial slice, the predicted damage by the shear anisotropic model is almost three times the value predicted by the HGO model and the coronal and the sagittal slices also show more damage (compare values at end of simulations in Fig. 6).

In addition to damage comparison, radial-circumferential shear strains are compared for the two models as shown in Fig. 7. For all orientations, the overall shear strains are higher in the shear anisotropic model (top row of each sub-figure) compared to the HGO shear strains (bottom row of each sub-figure). This observation is also mainly due to the difference in material properties between the shear anisotropic model and the HGO model.

DISCUSSION

Significant differences in resultant damage between the two models are evident, as shown in Fig. 5b.We note that most computational models show damage primarily at the boundaries between white and gray matters, due to the differences in stiffness between the two tissues. However, using the shear anisotropic model, some damage begins and remains in the deep white matter tissue, away from the boundaries between white and gray matters. This observation is supported by MRI studies on both animal and human injuries[21] and the work of Smith and Meaney[32] in which diffuse axonal injury was characterized to be deeper in the white matter.

We find it useful to examine the damage history, i.e. the progress of damage throughout all time-frames of the simulation. Figure 6 shows the damage predicted by the shear anisotropic (solid lines) and the HGO (dashed lines) models as a function of time. The damage in the axial slice was not only higher than the other cases but also developed over a longer time. This is consistent with the loading conditions, and more specifically the angular acceleration in the z direction (applied to the axial slice) which has the maximum magnitude compared to the other two directions (applied to coronal and sagittal slices). Nevertheless, the damage predicted by the HGO model stops evolving as soon as the loading is stopped at 15 ms while in the shear anisotropic model, the damage continued increasing until around 40 ms. This may be because of the slower shear wave speed in the shear anisotropic model (0.5 m/s compared to 2.4 m/s in the HGO model).

A comparison of the radial-circumferential shear strains reveals differences between the two models in addition to the damage differences. For the coronal and the sagittal slices, the shear anisotropic model predicts higher levels of shear strains (Figs. 7b and 7c) and damage in the brainstem. Such damage is not seen in the HGO simulation. Montgomery *et al.*[22] examined mild traumatic brain injury patients and found that the majority of the patients had abnormal brainstem function even after six weeks from the injury. Another study by Delano-Wood *et al.*[6] on veterans with chronic mild to moderate traumatic brain injury revealed a link between brainstem white matter integrity and the loss of consciousness after the injury. Due to the inclusion of shear anisotropy in the shear anisotropic model, the brainstem experiences higher shear strains which translate to higher predicted damage compared to HGO predictions (Fig. 5b). Note, however, that our simulations include only one family of fibers in each element.

Our simulations using our validated material model strongly suggest that considering shear anisotropy (addition of I_5) is important for computational predictions of mTBI. The injury predictions of the shear anisotropic model are significantly different than those predicted by the HGO model in terms of level of injury, location of injury and shear sensitivity. Although the injury threshold that we use is often used in the literature, we believe that more work is needed to correlate the symptoms presented by the injured subject with the predicted damage outcomes. Further, since the real fiber network of the brain has many crossing fibers, the shear anisotropic model needs to be improved to accommodate multiple families of fibers. Finally, we intend to extend this work for full 3D simulations of brain injury.

ACKNOWLEDGMENTS

The first author (FM) appreciates the support of Kuwait University through a scholarship. The second author (KTR) acknowledges support from the National Institute of Neurological Disorders and Strokes, National Institutes of Health (Project # R01NS055951). The authors also thank Dr. Andrew Knutsen and Dr. Dzung Pham from the Henry Jackson Foundation for sharing tagged-MRI experimental data from Knutsen *et al.*, J Biomechanics (2014). The authors also appreciate discussions and support from Dr. Shailesh Ganpule.

REFERENCES

1. Bain AC and Meaney DF Tissue-level thresholds for axonal damage in an experimental model of central nervous system white matter injury. J. Biomech. Eng. Trans. ASME 122:615–622, 2000.
2. Begonia M, Prabhu R, Liao J, Horstemeyer M, and Williams L. The influence of strain rate dependency on the structure-property relations of porcine brain. Ann. Biomed. Eng 38:3043–3057, 2010. [PubMed: 20505994]
3. Chatelin S, Deck C, Renard F, Kremer S, Heinrich C, Armspach JP, and Willinger R. Computation of axonal elongation in head trauma finite element simulation. J. Mech. Behav. Biomed. Mater 4:1905–1919, 2011. [PubMed: 22098889]
4. Cloots R, Van Dommelen J, Nyberg T, Kleiven S, and Geers M. Micromechanics of diffuse axonal injury: influence of axonal orientation and anisotropy. Biomech. Model. Mechanobiol 10:413–422, 2011. [PubMed: 20635116]
5. Colgan NC, Gilchrist MD, and Curran KM Applying dti white matter orientations to finite element head models to examine diffuse tbi under high rotational accelerations. Prog. Biophys. Mol. Biol 103:304–309, 2010. [PubMed: 20869383]
6. Delano-Wood L, Bangen KJ, Sorg SF, Clark AL, Schiehser DM, Luc N, Bondi MW, Werhane M, Kim RT, and Bigler ED Brainstem white matter integrity is related to loss of consciousness and postconcussive symptomatology in veterans with chronic mild to moderate traumatic brain injury. Brain Imaging Behav. 9:500–512, 2015. [PubMed: 26248618]

7. Donnelly B. and Medige J. Shear properties of human brain tissue. J. Biomech. Eng 119:423, 1997. [PubMed: 9407281]
8. DVBIC. Defense and veterans brain injury center: dod worldwide numbers for tbi. http://dvbic.dcoe.mil/dod-worldwide-numbers-tbi, 2018.
9. El Sayed T, Mota A, Fraternali F, and Ortiz M. Biomechanics of traumatic brain injury. Comput. Methods Appl. Mech. Eng 197:4692–4701, 2008.
10. Estes MS and McElhaney JH Response of brain tissue of compressive loading. In: The Fourth ASME Biomechanics Conference 1970.
11. Ganpule S, Daphalapurkar NP, Ramesh KT, Knutsen AK, Pham DL, Bayly PV, and Prince JL A three-dimensional computational human head model that captures live human brain dynamics. J. Neurotrauma 34:2154–2166, 2017. [PubMed: 28394205]
12. Holzapfel GA Nonlinear Solid Mechanics: A Continuum Approach for Engineering. Chichester, NY: Wiley, xiv, 2000.
13. Jin X, Zhu F, Mao HJ, Shen M, and Yang KH A comprehensive experimental study on material properties of human brain tissue. J. Biomech 46:2795–2801, 2013. [PubMed: 24112782]
14. Kimpara H, Nakahira Y, Iwamoto M, Miki K, Ichihara K, Kawano S, and Taguchi T. Investigation of anteroposterior head-neck responses during severe frontal impacts using a brain-spinal cord complex fe model. Stapp Car Crash J. 50:509–544, 2006. [PubMed: 17311175]
15. King AI, Yang KH, Zhang L, Hardy W, Center B, and Viano DC Is head injury caused by linear or angular acceleration? IRCOBI Conference—Lisbon (Portugal), 2003.
16. Kleiven S. Predictors for traumatic brain injuries evaluated through accident reconstructions. 51st Stapp Car Crash J., pp. 81–114, 2007.
17. Kleiven S. and von Holst H. Consequences of head size following trauma to the human head. J. Biomech 35:153–160, 2002. [PubMed: 11784533]
18. Knutsen AK, Magrath E, McEntee JE, Xing F, Prince JL, Bayly PV, Butman JA, and Pham DL Improved measurement of brain deformation during mild head acceleration using a novel tagged mri sequence. J. Biomech 47:3475–3481, 2014. [PubMed: 25287113]
19. Lanir Y. Constitutive-equations for fibrous connective tissues. J. Biomech 16:1–12, 1983. [PubMed: 6833305]
20. Legates DR and McCabe GJ Evaluating the use of “goodness-of-fit” measures in hydrologic and hydroclimatic model validation. Water Resour. Res 35:233–241, 1999.
21. Margulies SS and Thibault LE A proposed tolerance criterion for diffuse axonal injury in man. J. Biomech 25:917–923, 1992. [PubMed: 1639835]
22. Montgomery EA, Fenton GW, McClelland RJ, Macflynn G, and Rutherford WH The psychobiology of minor head-injury. Psychol. Med 21:375–384, 1991. [PubMed: 1876643]
23. Moriasi DN, Arnold JG, Van Liew MW, Bingner RL, Harmel RD, and Veith TL Model evaluation guidelines for systematic quantification of accuracy in watershed simulations. Trans. ASABE 50:885–900, 2007.
24. Nicolle S, Lounis M, and Willinger R. Shear properties of brain tissue over a frequency range relevant for automotive impact situations: new experimental results. Stapp Car Crash J. 48:239–258, 2004. [PubMed: 17230269]
25. Nicolle S, Lounis M, Willinger R, and Palierne JF Shear linear behavior of brain tissue over a large frequency range. Biorheology 42:209–223, 2005. [PubMed: 15894820]
26. Ning X, Zhu Q, Lanir Y, and Margulies S. A transversely isotropic viscoelastic constitutive equation for brainstem undergoing finite deformation. J. Biomech. Eng. Trans. ASME 128:925–933, 2006.
27. Prange MT and Margulies SS Regional, directional, and age-dependent properties of the brain undergoing large deformation. J. Biomech. Eng. Trans. ASME 124:244–252, 2002.
28. Rashid B, Destrade M, and Gilchrist MD Mechanical characterization of brain tissue in compression at dynamic strain rates. J. Mech. Behav. Biomed. Mater. 23–38, 2012.
29. Roberts JC, Harrigan TP, Ward EE, Taylor TM, Annett MS, and Merkle AC Human head-neck computational model for assessing blast injury. J. Biomech 45:2899–2906, 2012. [PubMed: 23010219]

30. Ruan JS, Khalil TB, and King AI Finite element modeling of direct head impact. Report 0148–7191, SAE Technical Paper, 1993.
31. Shugar TA and Katona MG Development of finiteelement head-injury model. J. Eng. Mech. Div. ASCE 101:223–239, 1975.
32. Smith DH and Meaney DF Axonal damage in traumatic brain injury. Neuroscientist 6:483–495, 2000.
33. Spencer AJM Deformations of Fibre-Reinforced Materials. Oxford: Clarendon Press, 1972.
34. Takhounts E, Eppinger R, Campbell J, Tannous R, Power E, and Shook L. On the development of the simon finite element head model. Stapp Car Crash J. 47:107–133, 2003. [PubMed: 17096247]
35. Tamura A, Hayashi S, Nagayama K, and Matsumoto T. Mechanical characterization of brain tissue in high-rate extension. J. Biomech. Sci. Eng 3:263–274, 2008.
36. Taylor PA and Ford CC Simulation of blast-induced early-time intracranial wave physics leading to traumatic brain injury. J. Biomech. Eng. Trans. ASME 131, 2009.
37. Velardi F, Fraternali F, and Angelillo M. Anisotropic constitutive equations and experimental tensile behavior of brain tissue. Biomech. Model. Mechanobiol 5:53–61, 2006. [PubMed: 16315049]
38. Ward C, Chang M, and Nahum A. Intracranial pressure—a brain injury criterion. In: 26th Stapp Car Crash Conference Proceedings SAE 801304, 1980.
39. Ward CC and Thompson RB The development of a detailed finite element brain model. In: Report 0148–7191, SAE Technical Paper, 1975.
40. Watanabe D, Yuge K, Nishimoto T, Murakami S, and Takao H. Development of a human head fe model and impact simulation on the focal brain injury. J. Comput. Sci. Technol 3:252–263, 2009.
41. Willmott CJ, Robeson SM, and Matsuura K. A refined index of model performance. Int. J. Climatol 32:2088–2094, 2012.
42. Wright RM, Post A, Hoshizaki B, and Ramesh KT A multiscale computational approach to estimating axonal damage under inertial loading of the head. J. Neurotrauma 30:102–118, 2013. [PubMed: 22992118]
43. Wright RM and Ramesh KT An axonal strain injury criterion for traumatic brain injury. Biomech. Model. Mechanobiol 11:245–260, 2012. [PubMed: 21476072]
44. Yao JF, Yang JK, and Otte D. Investigation of head injuries by reconstructions of real-world vehicle-versusadult-pedestrian accidents. Saf. Sci 46:1103–1114, 2008.
45. Zhang LY, Yang KH, and King AI Comparison of brain responses between frontal and lateral impacts by finite element modeling. J. Neurotrauma 18:21–30, 2001. [PubMed: 11200247]
46. Zhang LY, Yang KH, and King AI A proposed injury threshold for introduction mild traumatic brain injury. J. Biomech. Eng. Trans. ASME 126:226–236, 2004.
47. Zhou C, Khalil T, and King AI Shear stress distribution in the porcine brain due to rotational impact. In: 38th Stapp Car Crash Conference Proceedings SAE 942314, 1994.

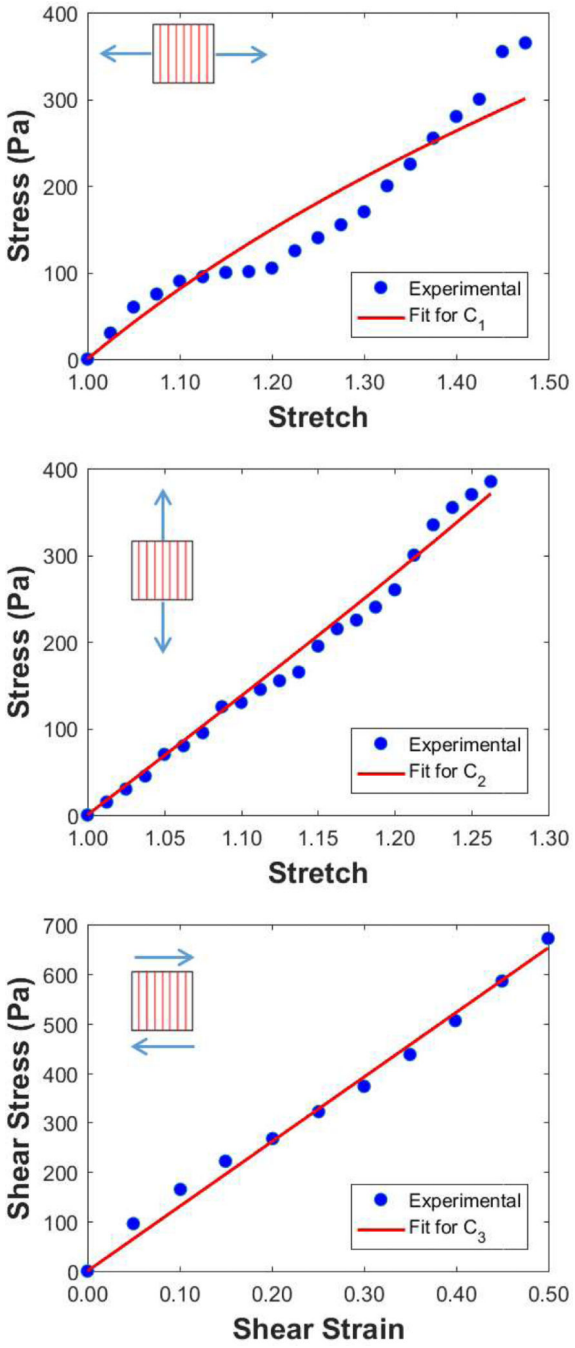

FIGURE 1.

Determination of the material parameters for the shear anisotropic model (Eq. 6). The first Piola–Kirchhoff (PK) stress is plotted vs. the corresponding stretch (top and middle), and vs. the shear strain (bottom). The experimental measurements are taken from the work of Velardi *et al.*[37] and Jin *et al.*[13] The fits allow us to obtain C_1 (top), C_2 (middle) and C_3 (bottom). Note: the relationship between the 1st PK stress (P) and the Cauchy stress σ (Eq. 8) is $J_\sigma = \mathrm{FP}^{\mathrm{T}}$.

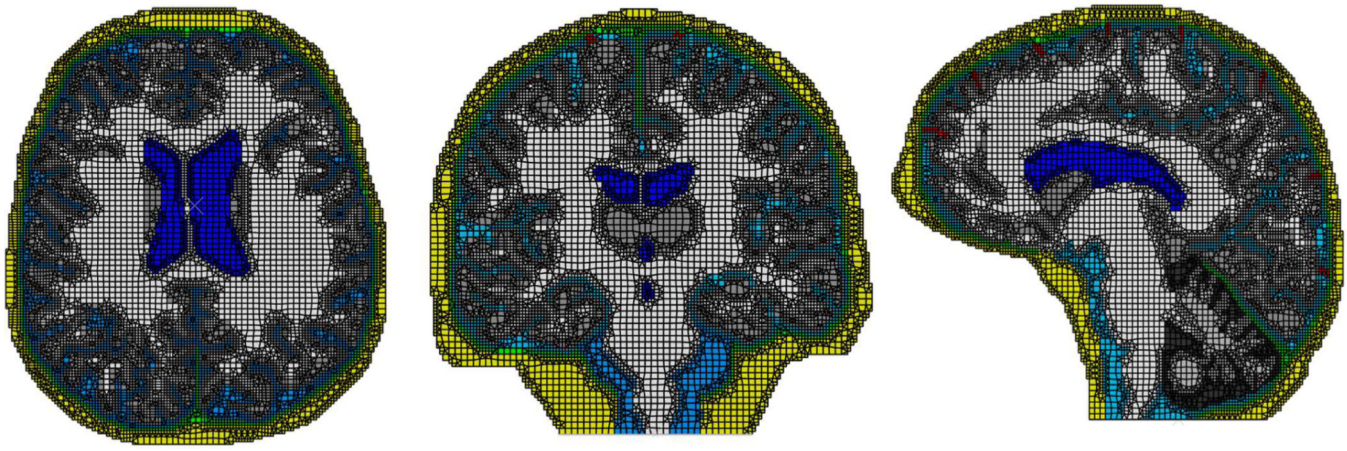

FIGURE 2.

The 2D finite element head models from the three representative planes: Axial (left), Coronal (middle) and Sagittal (right). The models include multiple brain structures that have been segmented from the MRI data.

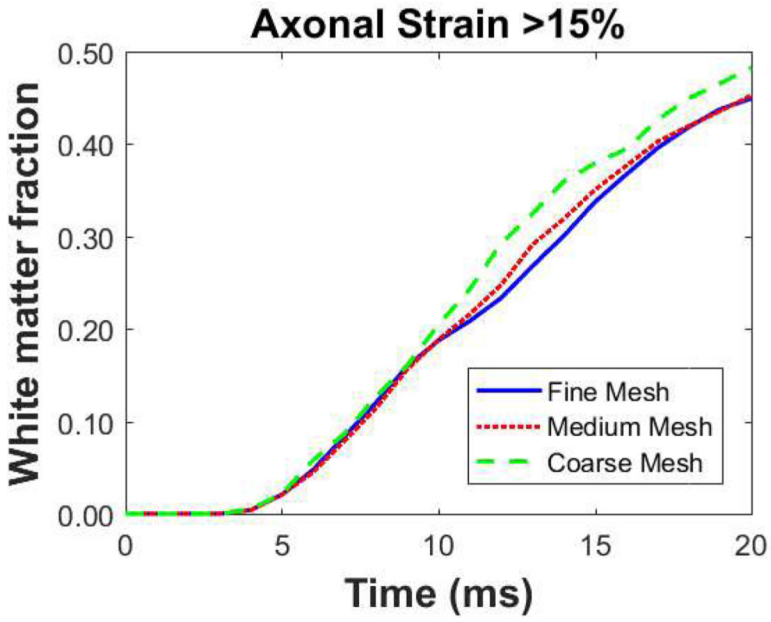

FIGURE 3.

Examination of mesh convergence in the shear anisotropic model for the particular case of the axial cross-section (we expect similar results for the other cross-sections). The evolution of white matter area fraction that sustains axonal strains greater than 15% is presented as a function of time for three mesh sizes: fine (max. element size = 1 mm), medium (max. element size = 2 mm) and coarse (max element size = 4 mm). The same analysis is performed for multiple axonal strain thresholds and all revealed similar results.

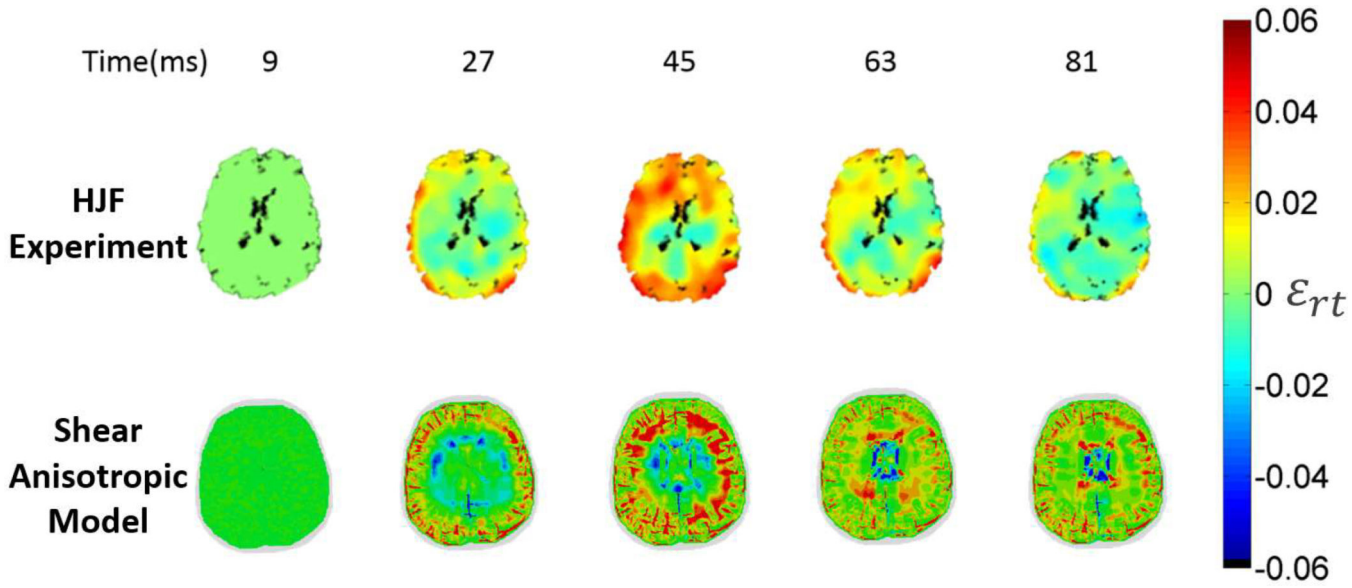

FIGURE 4.

Comparison of the measured (HJF) and the computed (shear anisotropic model) shear strain distributions for the axial cross-section for every 18 ms beginning 9 ms after loading. Note that the simulation resolution is higher than the experimental resolution, leading to the appearance of more detailed strain distributions in the model results. The HJF results are derived from the[18] paper.

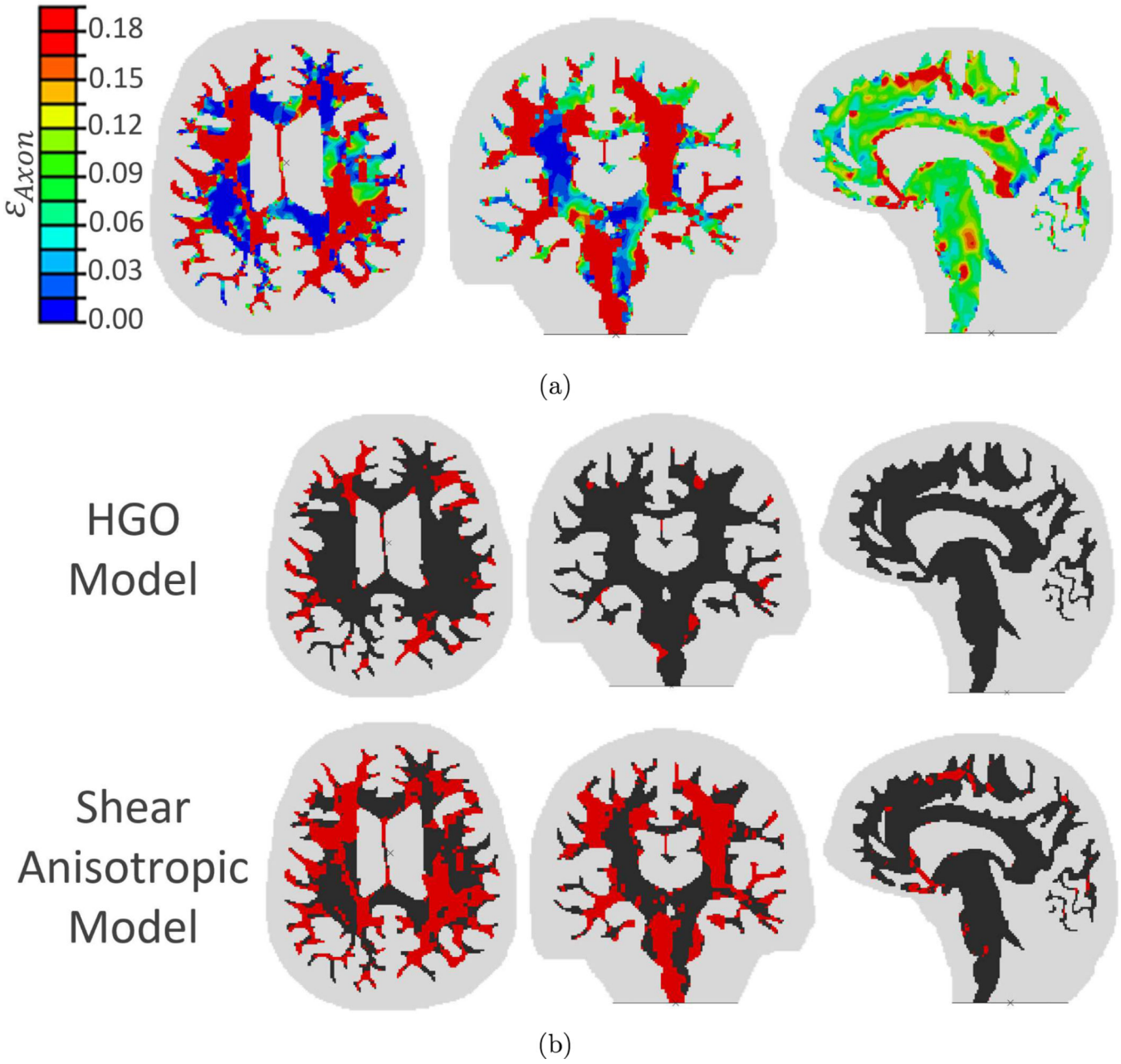

FIGURE 5.

Simulation results for: (a) The shear anisotropy of the injury case are presented in terms of the axonal strain (damage) distributions in the three cross-sections. Note: If axonal strain reached or exceeded the threshold of 18%, the element is labeled “damaged” for the remainder of the simulation. (b) The comparison of the injury predictions of the previous HGO model and the current shear anisotropic model. Damaged regions ($\varepsilon_{Axon} \geq 18\%$) in each slice shown in red for the axial (left), coronal (middle) and sagittal (right) orientations.

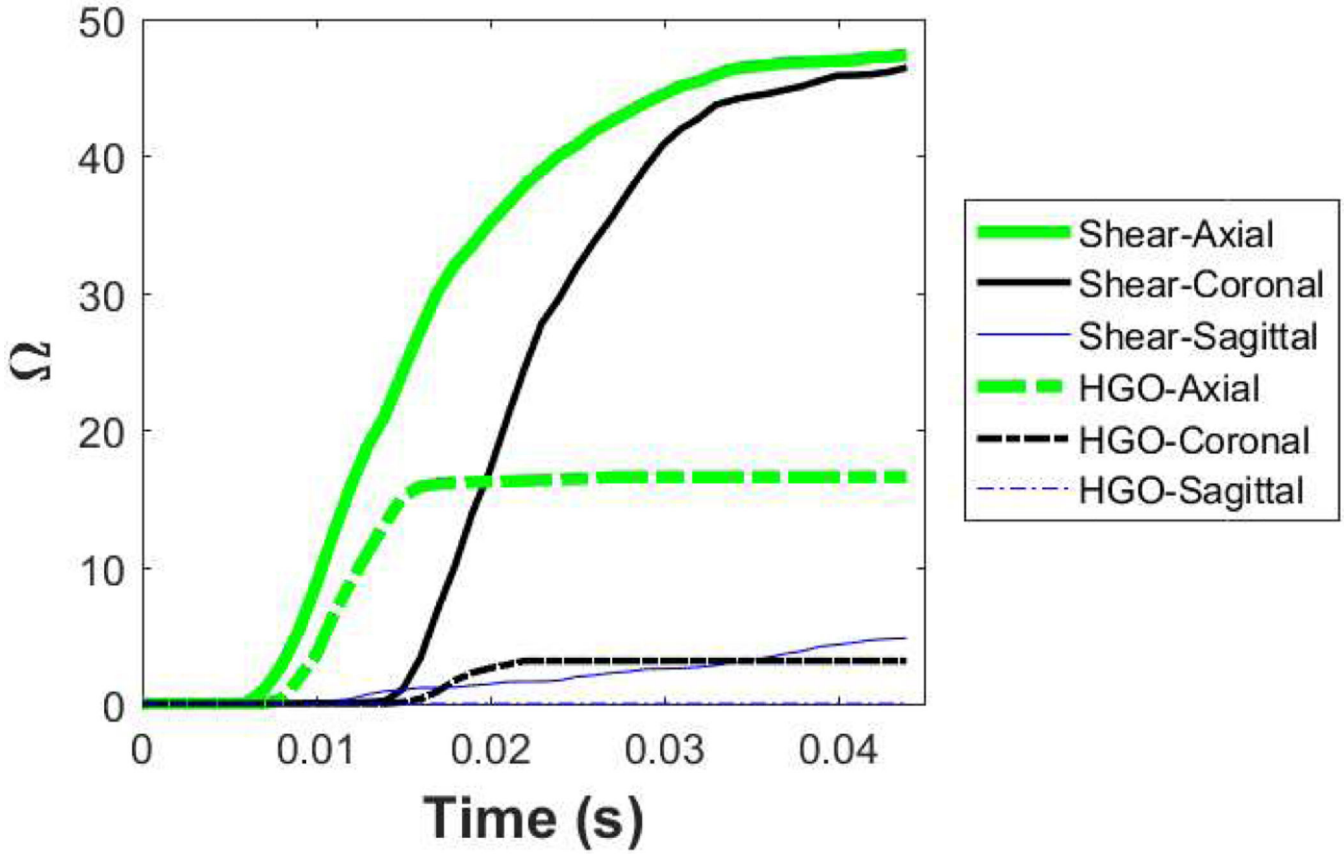

FIGURE 6.

Time evolution of the total damage predicted by the HGO and shear anisotropic models. Solid lines represent the shear anisotropic model and dashed lines represent the HGO model. Note the higher amounts of damage predicted by the shear anisotropic model.

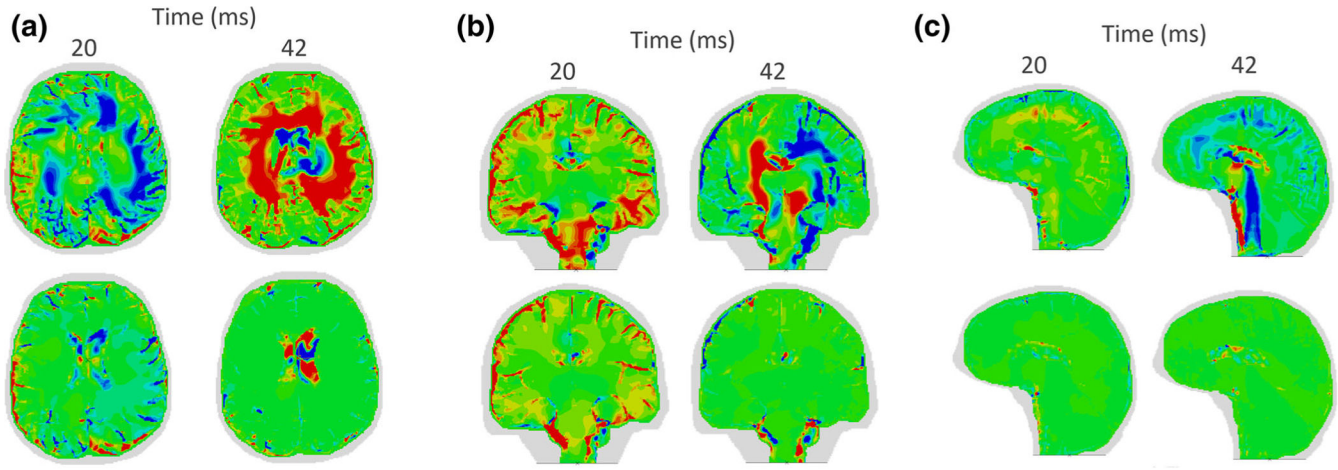

FIGURE 7.

Comparisons of the evolution of the radial-circumferential shear strains predicted by the shear anisotropic model (top row) and the HGO model (bottom row) in the (a) Axial (b) Coronal and (c) Sagittal orientations. Note the shear strain concentrations in the brainstem predicted by the shear anisotropic model in the coronal and sagittal cases.

TABLE 1.

Values for the material parameters in the shear anisotropic model (Eq. 6) determined by fitting the results of Velrdi *et al.*[37] and Jin *et al.*,[13] and in the HGO model (Eq. 9) used by Wright *et al.*[42]

	Shear anisotropic model	HGO model
C_1 (Pa)	148	3200
C_2 (Pa)	61	–
C_3 (Pa)	505	–
k_1 (Pa)	–	2716
k_2	–	0.0001
k	–	From DTI(0 – 1/3)

TABLE 2.

Material models used for the head structures other than white matter.

Material	Model	Equation
Cerebellum	NeoHookean	$W = C_1(\bar{I}_1 - 3) + \frac{K}{2}(J-1)^2$
Cerebrum and cerebellum	Viscoelastic	$\mu(t) = \mu_\infty + (\mu_0 - \mu_\infty)e^{-t\beta}$
Skull and dura	Linear elastic	E, υ
Bridging veins	1st-order Ogden	$W = \frac{\mu_1}{\alpha_1}\left(\overline{\lambda_1}^{\alpha_1} + \overline{\lambda_2}^{\alpha_1} + \overline{\lambda_3}^{\alpha_1} - 3\right) + \frac{K}{2}(J-1)^2$
CSF	Mie-Gruneisen EOS	$p = \frac{\rho_0 c_0^2 \xi}{(1-s\xi)^2}\left(1 - \frac{\Gamma_0 \varepsilon}{2}\right) + \Gamma_0 \rho_0 E_m, \xi = 1 - \frac{\rho_0}{\upsilon}$

The viscoelastic model is a one term Prony series defining the long-term and short-term shear moduli (μ_∞ and μ_0 respectively) and the decay constant β. Keep in mind that our model parameter C_1 is half the long-term shear modulus. The ratio of long-term to short-term moduli is kept the same as Wright et al.[42] The 1st-order Ogden model requires defining the shear modulus μ_1 and the dimensionless parameter α_1. The Mie–Gruneisen equation of state requires defining the reference density ρ_0, velocity constant c_0, two material constants s and Γ_0 and viscosity η.

TABLE 3.

Some measures of agreement between observations and predictions that can be used to assess TBI models.

Level of agreement test	Formula	Range	Agreement rating
Index of agreement d_r	$d_r = \begin{cases} 1 - \dfrac{\sum\lvert O_i - P_i\rvert}{2\sum\lvert O_i - \bar{O}\rvert} & \text{if} \quad \sum\lvert O_i - P_i\rvert \le 2\sum\lvert O_i - \bar{O}\rvert \\ \dfrac{2\sum\lvert O_i - \bar{O}\rvert}{\sum\lvert O_i - P_i\rvert} - 1 & \text{if} \quad \sum\lvert O_i - P_i\rvert > 2\sum\lvert O_i - \bar{O}\rvert \end{cases}$	− 1 to 1	↑ d_r ≡ better agreement
Coefficient of efficiency (E_2)	$E_2 = 1 - \dfrac{\sum\lvert O_i - P_i\rvert^2}{\sum\lvert O_i - \bar{O}\rvert^2}$	− ∞ to 1	↑ E_2 ≡ better agreement
RMSE to observations			
Standard deviation ratio (RSR)	$\mathrm{RSR} = \dfrac{\sqrt{(O_i - P_i)^2}}{\sqrt{\sum(O_i - \bar{O})^2}}$	0 to ∞	↓ RSR ≡ better agreement
Correlation score (CS)	$CS = (1 - \lvert NISE\rvert) \times 100$ $NISE = 1 - \dfrac{2\sum O_i P_i}{\sum O_i^2 + \sum P_i^2}$	0–100	86–100 excellent 65–86 good 44–65 fair 26–44 marginal 0–26 unacceptable

TABLE 4.

The degree of agreement between the shear anisotropic model and the HJF experiment at four specific times, using the measures described in Table 3.

Time (ms)	27	45	63	81
d_r	0.42	0.23	0.28	0.29
E_2	− 0.28	− 0.98	− 0.73	− 0.66
RSR	1.13	1.40	1.31	1.29
CS	53.70	47.16	39.44	42.29